Nanomed J. 11(2): 187-195, Spring 2024

RESEARCH PAPER

Green synthesized silver nanoparticles using *Rhazya stricta* extract for delivery of HDAC inhibitor panobinostat in MDA-MB-231 breast cancer cell line

Tayyaba Nawaz [1], Adeeb Shehzad [1]*, Waheed Miran [2], Aroosa Younis Nadeem [1], Tooba Nawaz [3]

[1]Department of Biomedical Engineering and Sciences, School of Mechanical and Manufacturing Engineering (SMME), National University of Sciences and Technology (NUST), Islamabad 44000, Pakistan
[2]Department of Chemical Engineering, School of Chemical and Materials Engineering National University of Sciences and Technology (NUST), Islamabad 44000, Pakistan
[3]Department of Gynecology and Obstetrics, Shaikh Zayed Hospital, Lahore, Pakistan

ABSTRACT

Objective(s): Concerns regarding increased breast cancer cases worldwide have spurred interest in the discovery of novel approaches to overcome this deadly disease. Although several treatment strategies have been developed to treat breast cancer including chemotherapy, an efficient drug delivery system remains a challenge. Here, we study the drug distribution and boosting the efficiency of Panobinostat, a histone deacetylase inhibitor, by using silver nanoparticles as a controlled drug delivery system.

Materials and Methods: Green synthesis of silver nanoparticles, as nanocarriers for drug delivery was synthesized by using Rhazya stricta extract and loaded with the drug. These drug-loaded nanoparticles were characterized by UV-vis spectroscopy, XRD, FTIR, SEM, and EDX techniques.

Results: The AgNPs had an average size of 20 nm and were stable over a period. The evaluation of drug encapsulation effectiveness and drug release capacity revealed 56% encapsulation efficiency and sustained drug release. The kinetics study of drug release showed the first-order reaction which means that drug concentration is proportional to drug release. The MTT assay showed that drug-loaded AgNPs had a potent and dose-dependent anticancer activity on the breast cancer cell lines (MDA-MB-231).

Conclusion: As the successfully green synthesized Panobinostat-AgNPs were stable and exhibited increased *in vitro* anticancer activity compared with free Panobinostat, our data demonstrate that the combination of AgNPs with Panobinostat improves the drug's long-term viability, effectiveness, and active targeting as a potential targeted therapeutic molecule for the treatment of cancer. To strengthen the utilization of this combination therapy in cancer therapy trials, further research is warranted *in vivo.*

Keywords: *Breast cancer, Drug delivery, Nanotechnology, Panobinostat, Silver nanoparticles*

How to cite this article
Nawaz T, Shehzad A, Miran W, Nadeem AY, Tooba Nawaz. Green synthesized silver nanoparticles using Rhazya stricta extract for delivery of hdac inhibitor panobinostat in mda-231 breast cancer cell line. Nanomed J. 2024; 11(2): 187-195. DOI: 10.22038/NMJ.2024.75733.1839

INTRODUCTION

Cancer is a very serious public health problem and it is estimated that cancer cases will rise to 20 million annually in the next decade globally [1]. Among all categories of cancer, breast cancer has the highest ratio worldwide. Traditional methods for breast cancer treatment include surgery, chemotherapy, and radiotherapy [2], among which chemotherapy has been widely used in clinics because of its quick and easy procedure. However, chemotherapy-based cancer treatment still comes with some serious risks. For instance, it is less effective in halting the growth, spread, and recurrence of tumors because the drugs are randomly distributed throughout the body and susceptible to multidrug resistance while being used [3-5]. Also, chemotherapeutic drugs are mostly hydrophobic, thus they need to be delivered in higher concentrations to attain the desired results. Higher concentrations lead to more toxicity and damage to healthy tissues causing adverse reactions [6, 7]. Thus, designing an effective drug delivery system that can enable drug delivery to the tumor cells with no side

* *Corresponding author: Email: adeeb.shehzad@smme.nust.edu.pk*
Note. This manuscript was submitted on October 20, 2023; approved on December 30, 2023

effects is high in demand [8].

Nano-delivery systems, a relatively new but rapidly developing area of study, utilize materials in the nanoscale range to deliver therapeutic drugs to specific targeted regions in a controlled manner. Recent years have witnessed several significant applications for the use of nanomedicine in the treatment of various diseases including breast cancer [9-11]. The development of nanoparticles as drug carriers proved beneficial for therapeutic purposes, i.e., targeted drug delivery, higher bioavailability, and lower toxicity [12]. Nanotechnology has made cancer therapy safer and more effective. This innovative approach is an encouraging strategy to deliver anti-cancerous drugs directly to the tumor cell and thus it doesn't damage the healthy cells. Other than that, nanoparticles can improve the stability of the drug as well as the accumulation of drugs in the tumor [13-16].

Silver nanoparticles (AgNPs) possess anti-microbial and anti-cancerous properties such as anti-proliferation and induction of apoptosis and thus can be used effectively against cancer [17]. AgNPs can be synthesized through chemical, physical, and biological methods. In the physical method, it becomes challenging to control the size of particles also this method is not very cost-effective. In chemical methods, chemicals may prove more toxic than effective against the cells. The biological method is an efficient strategy for the synthesis of silver nanoparticles through plant extracts as it gives greater output with lesser cost [18, 19].

In this study, AgNPs are synthesized from the *Rhazya stricta* extract based on low cost and easy availability. *R. stricta* plant, also known as "Harmal", belongs to the family *Apocynaceae* and is located widely in South Asia [20]. It is called "Rangobul" in Urdu and "Vergalum" and "Ganderi" in Pushto. "Harmal" is the term used in Arabic. But it's important to distinguish clearly between the harmal related to *R. stricta* and the harmal associated with *Peganum harmala* [21]. It has several medicinal advantages as it has anti-microbial, anti-oxidant, and anti-cancerous properties [22]. *R. stricta* has a high concentration of alkaloids, with more than 50 distinct alkaloids having been discovered from the plant. The primary alkaloids comprise ajmalicine, catharanthine, vindoline, and voacangine [23]. Another significant class of secondary metabolites present in *R. stricta* are flavonoids. The plant contains a diverse range of flavonoids, containing flavonols, flavones, and flavanones. Flavonoids possess notable antioxidant and anti-inflammatory characteristics. Tannins have antioxidant and antibacterial properties due to their astringent nature, whereas terpenoids, including triterpenoids and sesquiterpenoids, provide a wide range of biological advantages. The secondary metabolites of *R. stricta* exhibit considerable potential for medicinal uses [24-26]. These compounds are responsible for the silver ions reduction and thus the synthesis of silver nanoparticles. Silver nanoparticles synthesized by *R. stricta* can prove effective therapeutic agent against cancer because of its wide range of biological activities [27, 28].

HDAC inhibitor (HDACi) is a class of anti-cancerous agents that removes the acetyl group from core histones and thus relaxes the structure of chromatin [29]. HDAC inhibitors possess epigenetic roles including cell cycle arrest, apoptosis, and cell death. However, HDACi has distribution and rapid clearance problems when delivered in free form [30-32]. Panobinostat is an FDA-approved HDACi that alter the transcriptional activity, damages DNA, and express those proteins that cause apoptosis of cell [33]. However, it has several delivery challenges, i.e., it is problematic to administer it in free form and pharmacokinetic properties show that it is rapidly cleared from tissues [34-36].

The ability to combine silver nanoparticles' anticancer characteristics with the pharmacological action of an HDAC inhibitor could be the key to treat cancers that have stopped responding to chemotherapy and radiotherapy. Assessing the possibility of using AgNPs to deliver Panobinostat to the tumor site, where the silver nanoparticles then release the drug and start to act against cancer cells after being uptaken by the tumor cells, this is a viable cancer treatment technique [37]. This study will investigate the use of silver nanoparticles as a target-specific drug delivery vehicle for HDAC inhibitor Panobinostat with the hypothesis that entrapment within a Nano-carrier that is capable of sustained release will prove beneficial for its usage in cancer treatment when applied to human breast cancer cell lines MDA-MB-231.

The focus on cytotoxicity in research arises from its immediate and quantifiable characteristics in contrast to HDAC inhibition. Utilizing cell viability assays enables a rapid and quantitative assessment of the effect of a chemical on cell proliferation and viability, offering essential information about its therapeutic capacity and informing future research. While HDAC inhibition may not always have a consistent link with cytotoxicity, cytotoxicity itself is a more dependable measure. Certain HDAC inhibitors demonstrate cytotoxic effects, while others do not. The correlation between HDAC inhibition and cytotoxicity depends on factors

such as the kind of cell and the specific HDAC inhibitor being utilized. By prioritizing cytotoxicity as the main measure, we may more accurately evaluate the effectiveness of a molecule and make informed decisions on its potential for medicinal development.

MATERIALS AND METHODS

Chemicals

Silver Nitrate (Sigma Aldrich), Xylitol (Sigma Aldrich), Methanol (Sigma Aldrich), Panobinostat (Solarbio Life Science), Whatman filter paper (125 mm), Dimethyl sulfoxide (DMSO), MTT assay reagent 3-(4,5-dimethylthiazal-z-yl)-2,5-di-phenylterazolium, Phosphate Buffer Solution (PBS), and Deionized water were used.

Collection of plant

R. Stricta roots were chosen for their low cost, easy availability, and good medicinal properties. *R. stricta* were purchased from the Nursery farm, in Islamabad and washed with distilled water to remove impurities. Roots were cut down into small parts and dried in sunlight (in the winter season) for 2-3 weeks. Once roots were completely dried, they were ground in a grinder and converted into powder form.

Plant extract preparation

The schematic for plant extract preparation is shown in Fig. 1. The powder of dried roots was 90 g which was soaked in 70% absolute methanol for 4-5 days at room temperature. It was filtered using Whattman filter paper. The methanol was then evaporated by using a rotary evaporator. After evaporation, the sample was dried by keeping it in a lab oven at 40 °C until it was completely dried. The final plant extract was used for the reduction and stabilization of silver nanoparticles.

When preparing plant extracts to reduce and stabilize silver nanoparticles, oven drying is a practical solution for various subtle reasons. The plant extract, which is essential for the synthesis process, has a special function of reducing and stabilizing silver nanoparticles, making the possible loss of heat-sensitive chemicals less significant. The thermolabile components are minimally essential for achieving the defined target of the plant extract's reduction and stabilization process. Moreover, the utilization of oven drying offers benefits compared to freeze-drying because of its simplicity and cost-efficiency, which are crucial considerations in the context of producing plant extracts on a big scale. The use of a moderate drying temperature (40 °C) for oven drying is a safe choice, as it reduces the probability of substantial degradation in the plant extract.

Silver nanoparticles synthesis and drug loading

AgNPs were synthesized by reducing Ag+ ions using *Rhayza Stricta* root extract as a reducing agent. 10 g dried plant extract was dissolved in 18 ml methanol. In an Erlenmeyer flask, a solution of Silver Nitrate was prepared with a molarity of 1 mM, by dissolving 0.017 g of silver nitrate in 100 ml of deionized water. 3 ml plant extract was dissolved dropwise in the 50 ml silver nitrate with continuous shaking. 3 mL xylitol was also added to the beaker to prevent agglomeration. The mixture was stirred at 60 °C for 1-2 hr on a hot plate by using a magnetic stirrer. The color of the mixture was changed from yellowish to dark brownish color, which confirmed the reduction of (Ag+) into (Ag0) and thus the synthesis of silver nanoparticles. Next, the stock solution of drug Panobinostat was prepared in the DMSO at the concentration of 10 mg/ml. The drug was conjugated with silver nanoparticles through covalent bonding. The

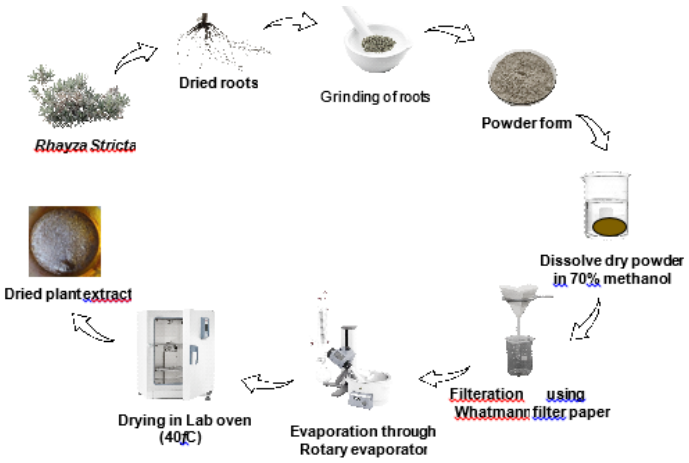

Fig. 1. A schematic showing preparation of *Rhayza Stricta* root extract.

samples obtained were employed for further testing.

Characterization of blank AgNPs and AgNPs conjugated with drug

The sample was centrifuged at 12,000 rpm for 20 minutes. Then particles were sonicated by using a water bath sonicator which is used for evenly dispersing nanoparticles. Nanoparticles were employed for further characterization. The reduction of silver ions to silver nanoparticles and conjugation of drug onto nanoparticles was studied using a UV-visible spectrophotometer at wavelengths ranging from 300-700 nm. The UV analysis of silver nanoparticles, drug, and drug-loaded AgNPs was performed in the Perkin Elmer Spectrophotometer. The sample of nanoparticles was diluted in methanol while a sample of nanoparticles and drug was diluted in DMSO. The cuvette was filled with 50 µL of each suspension and used to measure the UV-Vis absorption spectra. To prove Beer's law, i.e., absorbance is directly proportional to the concentration allowing the absorbance of a solution to be measured to determine the concentration of the solution. UV was performed at different concentrations of nanoparticles, i.e., 325 µL, 275 µL, 225 µL, 175 µL, and 125 µL.

Analysis of functional groups, molecular structure, and chemical bonding of samples was done using FTIR spectroscopy. The Fourier-transform infrared spectroscopy (FTIR) Perkin Elmer, Spectrum 100, was used to find out the functional chemical groups coupled with plant extract, AgNPs, drug, and silver nanoparticles loaded with the drug. The samples were measured in the range of 500–4000 $cm^{-1.}$ The process involved distributing a sample in KBr and then gently mixing it.

X-ray powder diffraction was used for determining the crystallinity of samples. STOE Germany, model Theta-Theta S/N 65022 is used for XRD analysis and glass slides of respective samples were prepared.

The size and morphology of the material were studied using a scanning electron microscope (SEM). SEM JEOL Japan, model JSM-6490A, was used to examine the morphological characteristics of blank silver Nanoparticles and silver nanoparticles conjugated with the drug. Glass slides were prepared by adding drops of sample on a slide and drying them through vacuum drying. By putting the sample on a carbon-coated copper grid, the electron microscopic pictures were taken of the sample's thin layers. Energy Dispersive X-ray analysis was used to determine the presence of elemental silver and drug in silver nanoparticles and drug-loaded AgNPs respectively.

Drug loading efficiency

Silver nanoparticles and free drugs were separated by centrifugation at 13,000 g for 1 hr. With the use of a UV-visible spectrophotometer and a calibration curve based on the weight percentage of the original drug to the free drug in the supernatant, the concentration of Panobinostat in nanoparticles was measured by determining the absorbance at 290 nm. The following equation was used to obtain the entrapment efficiency given as a percentage:

$$Encapsulation\ efficience = \frac{Total\ drug\ added - free\ drug\ in\ the\ supernatant}{Total\ drug} \times 100$$

Drug release

Using a dialysis technique, drug release from nanoparticles was investigated. To remove the preservative, dialysis bags were completely rinsed in distilled water after soaking in distilled water at room temperature for a few minutes before use. Panobinostat was released *in vitro* from silver nanoparticles using phosphate-buffered saline dialysis in a dialysis sac (PBS; pH 7.4). Over eight hours, samples were taken every half-hour, and their drug amount was measured by using a spectrophotometer at 290 nm.

Kinetic analysis of the drug release

A key aspect in establishing a drug's therapeutic potential is the process through which the molecule is released from the matrix. Various kinetic models have been applied to *in vitro* release study and AgNPs permeability to elucidate the process of drug release from AgNPs. The release date was then fitted into kinetic mathematical equations (i.e., zero order, first order, Korsmeyer-Peppas and Higuchi models).

In vitro analysis/anticancer activity

The MTT assay (3-(4, 5-dimethylthiazol- 2-yl)-2, 5-diphenyltetrazolium bromide) was used to determine the cell cytotoxicity. MDA-MB-231cells were plated in a 96-well plate (1x104 cells/well) and given the night for adherence. After 24 hours, a fresh medium with differently concentrated (0, 20, 30, 50, 100, 150 nM) Panobinostat-AgNPs and Panobinostat were aspirated. For 24 hours, the plate was left intact in the incubator. MTT solution was applied to every single well and kept for incubation for 4 hours. The supernatant was removed after 4 hours, and 100 µL of dimethyl sulfoxide (DMSO) was added to the purple formazan to dilute it. In an ELISA plate reader, the plate was read at 570 nm. The percentage of cell cytotoxicity was determined by using the optical density.

$$Percentage\ cell\ viability = \frac{Value\ of\ OD\ (treatment)}{Value\ of\ OD\ (control)} \times 100$$

One-way ANOVA with a significant P-value < 0.05 was used to statistically analyze all the data, which were then given as mean ± SD.1

RESULTS AND DISCUSSION

Green synthesis of nanoparticles and its characterization

Visual analysis was used initially to confirm the green synthesis of silver nanoparticles using *R. stricta* extract. The reaction mixture first had a pale-yellow appearance, and when it turned into a brown color, it indicated the synthesis of silver nanoparticles. After 1-2 hr the reaction mixture turned dark brown indicating that the reduction of the silver ion process was complete (Fig. 2A). The prepared nanoparticles were stable for 2 months and not aggregated because of xylitol.

The conduction band and the valence band in AgNPs are quite close to one another, and the electrons there are unrestrained [38]. When the AgNP electrons are activated by visible light at particular wavelengths, they collectively oscillate, creating a surface plasmon resonance band that gives rise to these free electrons [39]. The surface plasmon resonance band is related to the wavelength at which the max peak absorbance occurs [40]. The wavelength of silver nanoparticles often falls between 380 and 450 nm. Our characteristic peak for silver nanoparticles lies at ~420 nm (Fig. 2B). On the green synthesis of AgNPs, a similar outcome was reported earlier [41]. Beer's law was also proved by taking Spectrophotometer measurements of five nanoparticle concentrations in methanol and linear dependency is shown in Fig. 2C (inset). From these absorption spectra, a linear curve of the absorbance and concentration was plotted which proves that absorbance is directly proportional to concentration.

In the present experiment, an FTIR analysis was employed to detect phytochemicals contained in *R. stricta* extract which is an agent for reducing the silver ions to silver nanoparticles. The FTIR of *R. stricta* extract, AgNPs, free Panobinostat,

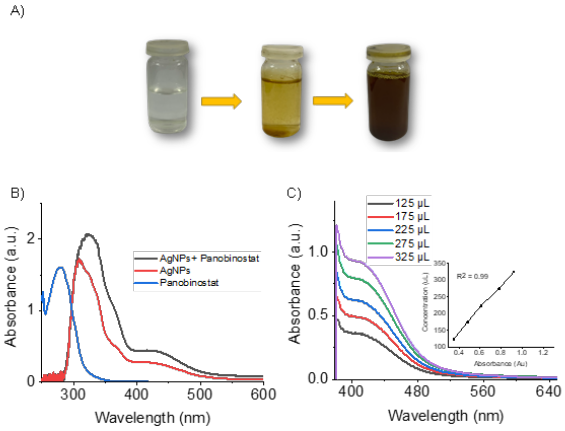

Fig. 2. (A) Visual observation of AgNPs synthesis (B) UV–Vis spectra of AgNPs, Panobinostat, and Pb-AgNPs (C) Concentration-dependent UV-vis absorption spectra of nanoparticles

and Panobinostat-AgNPs are presented in Fig. 3A. FTIR results revealed the successful conjugation of Panobinostat on AgNPs. The spectrum shows the characteristic bands at 3419, 2989, 2050, 1626, 1012, and 696 cm^{-1}. *R. stricta* extract showed a peak at 3410 that indicates the stretching of the N-H bond of the amine group. Peak 2859 shows the stretching of the C-H bond of a methyl group, peak 1625 indicates the C=C bond of the alkene group, peak 1012 shows the C=O bond, the peak 696 indicates the ring of plane aromatic band. Silver nanoparticles showed a peak at 1626 cm^{-1} corresponding to C=O symmetric stretching in the AgNPs. The stretching of the N–H bond of the Panobinostat was displayed by the band at 3410 cm^{-1}. Absorption bands at 1626 cm^{-1} and 1012 cm^{-1} represent a C=C and C=O, respectively, and the band at 2989 cm^{-1} was allotted to the C–H stretching vibration. The Panobinostat-AgNPs exhibited bands at 3350 cm^{-1}, which corresponded to the stretching vibration of the O–H group, and the band at 1626 cm^{-1} denoted strong C=C stretching. The stretching bands at 3419 cm^{-1} of the N–H bond of the Panobinostat moved to 3442 cm^{-1} for the Panobinostat-AuNPs, presenting conjugation of Panobinostat on AgNPs. The associated N-H peaks' broadening and shift to

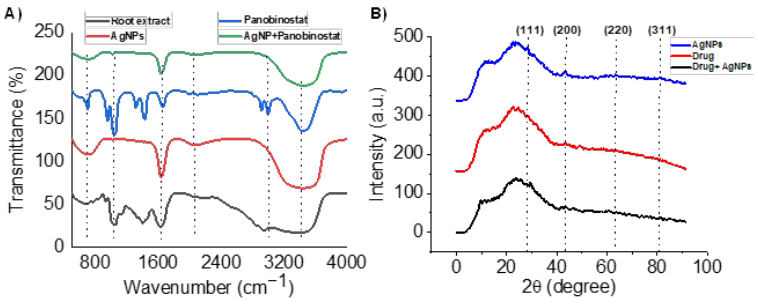

Fig. 3. (A) FTIR spectrum of *R. stricta* root extract, AgNPs, Panobiostat, and Pb-AgNPs. (B) XRD analysis showing the crystalline nature of silver nanoparticles, Panobinostat, and Pb-AgNPs

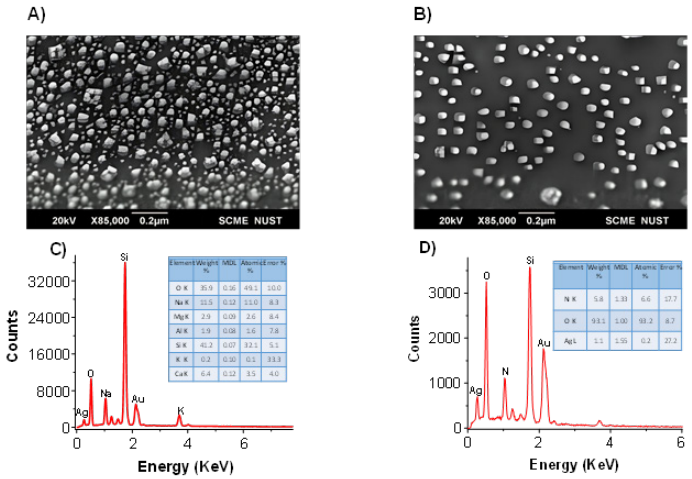

Fig. 4. Scanning Electron Microscopy (SEM) (A) AgNPs (B) Pb-AgNPs and EDX analysis of (C) AgNPs (D) Pb-AgNPs

higher wavelengths served as evidence that the drug has coupled to the surface of AgNPs.

The AgNPs, Drug, and Drug loaded AgNPs samples' crystallinity was confirmed by XRD analysis. By recording the XRD from 0° to 100°, the crystalline nature of the samples was assessed. The 2θ angles and related Miller indices (hkl which indicates a normal to the planes in the basis of the primitive reciprocal lattice vectors planes) are given in Fig. 3B. They were indexed to the Joint Committee on Powder Diffraction Standards (JCPDS) standard planes of crystalline samples with face-centered cubic structure. For the development of AgNPs, the (200) orientation is the preferable one. The bioorganic compounds used in the production of AgNPs may be responsible for other peaks. The Debye-Scherrer equation (D = k/cos) was used to determine the nanoparticles' sizes. It was determined that the typical crystalline size was about 20 nm.

The synthesized silver nanoparticles and the drug-loaded silver nanoparticles' morphological characteristics and size details were shown by SEM images taken at 10 kV. SEM images showed nanoparticle sizes in the 20-nm range (Fig. 4A and B). The result demonstrates that the synthesized AgNPs have spherical shapes. The figure shows that there is no agglomeration and that the synthesized AgNPs are well separated. Energy Dispersive X-ray shows the composition of silver nanoparticles and drug-loaded onto nanoparticles is visible in the spectrum. Fig. 4C and D illustrate different elemental compositions comprising Ag, O, Na, and Mg at different binding energies. Other smaller peaks, including Al, K, and Ca, were seen at different degrees of absorption energy. In Fig. 4C and D the loading of drug onto AgNPs was confirmed by the presence of N, O, and Ag.

Drug loading efficiency and drug release

Surface adsorption is the underlying concept of drug loading on silver nanoparticles [42]. When 0.5 mg drug was added to AgNPs, the % drug loading was 56%. The time-dependent mean of percentage drug release is shown in Fig. 5 which reveals the percentage cumulative drug release at time intervals of 30 min (PH 7.4).

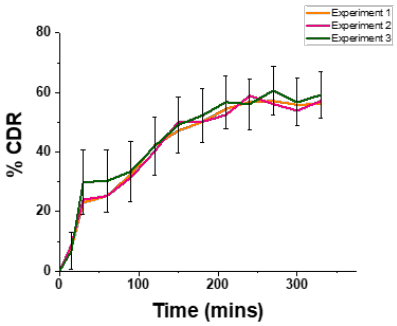

Fig. 5. Percentages of cumulative drug release (CDR) from silver nanoparticles of Panobinostat at definite time intervals

When it comes to drug release, the first stage may be crucial for the treatment of a disease since the drug is released quickly, and the slow-release phase may cement the therapeutic effect. Through two rounds of release, drugs will play a bigger part in the healing process.

The rate of drug release values calculated for kinetic models are shown in Table 1. The first-order release model and the Higuchi Model equation provided the best description of the

Table 1. The different kinetic models on drug release (pH 7.4)

Model name	Equation	R^2
Zero-order	$Q = Q + kt$	0.8408
First-order	$\log Q = \log Q_0 - kt/2.303$	0.8943
Higuchi	$Q = k\,t^{1/2}$	0.9584
Hixon- Crowell	$Q_0^{1/3} - Qt1/3 = kt$	0.8786

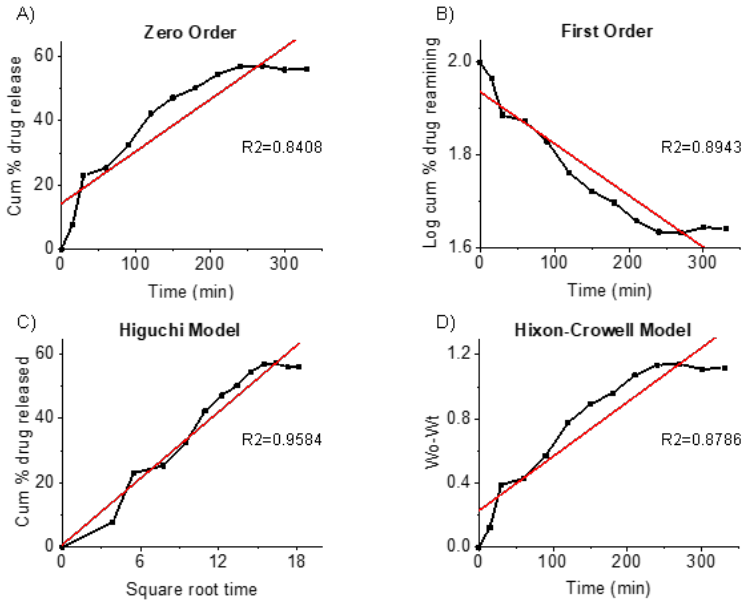

Fig. 6. Fitting drug release data to multiple kinetic models (A) Zero order (B) First order (C) Higuchi model (D) Hixson-Crowell model obtained from the dissolution studies of the drug-loaded nanoparticles

drug release kinetics of this formulation (Fig. 6). The R^2 value of the first-order model is close to 1 and demonstrated drug release via membrane diffusion. The first-order reaction showed that the release of Panobinostat from Panobinostat-AgNPs depends on concentration. Because the network structure of the nanoparticles is stable at this pH, the drug release was rather slow. The initial burst release will serve as a loading dose to stop the spread of the disease, and the continuous release phase will help provide a more effective therapeutic result [43].

MTT assay

MTT assay findings for Panobinostat, and Panobinostat-AgNPs at various concentrations are presented in Fig. 7. The impact of Panobinostat-AgNPs on the viability and growth of breast MDA-231 cells was evaluated using the MTT test. We've shown that the MDA-MB-231 breast cell line is sensitive to the cytotoxic effects of Panobinostat, and Panobinostat-AgNP. Panobinostat, and Panobinostat-AgNP concentrations (0, 20, 30, 50, 100, and 150 nM) were tested in the current investigation, and the ability to inhibit MDA-MB-231 cells was dose-dependent. The evident result of increasing the concentration of AgNPs with Panobinostat is a reduction in cell viability. The MDA-MB-231 cell viability was reduced after the cells were treated with Panobinostat-AgNPs, and a larger cell cytotoxicity rate was observed with greater Panobinostat-loaded AgNPs. According to the viability assays, Panobinostat-

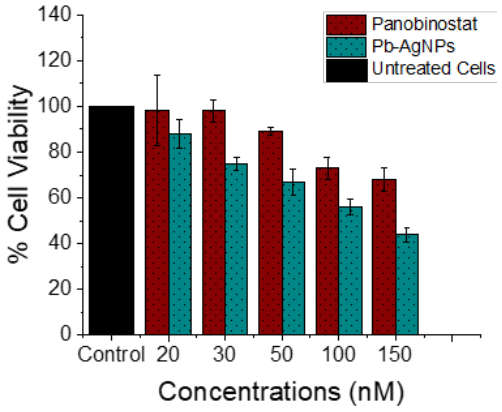

Fig. 7. *In vitro* cell viability of Panobinostat, Pb-AgNPs against breast cancer MDA-MB-231 cells after incubation of period 24 hr. The results of three separate trials were presented as mean ± SD. One-way ANOVA was used to statistically assess the results (*P< 0.05)

AgNPs dramatically reduced cell viability at various concentrations, which is similar to the combined cytotoxicity of Panobinostat and AgNPs. The size, charge, and form of the nanoparticles may have a role in MDA-MB-231's susceptibility to Panobinostat-AgNPs. Target cell cytotoxicity caused by nanoparticles has been linked to several mechanisms, including particle-induced apoptosis [42].

CONCLUSION

It was discovered in the current study that the Panobinostat loaded in silver nanoparticles was successfully prepared for targeted drug

administration and that there is a chance of developing a simple, eco-friendly, and novel Panobinostat-loaded AgNPs with a considerable drug loading efficiency. Furthermore, an *in vitro* release analysis with an efficient release profile and diffusion model demonstrated Panobinostat-AgNPs' considerable cytotoxicity when compared to Panobinostat, which is commercially available. All of these characteristics improve the pharmacokinetic profile, effectiveness, and active targeting of nanoparticles as a possible targeted therapeutic molecule in the treatment of cancer. The green synthesized AgNPs are a potential controlled drug delivery system and a sustained release mechanism for Panobinostat. Further *in vivo* testing of these findings is required.

FUNDING

The authors received no specific funding for this work.

CONFLICTS OF INTEREST

There is no conflict of interest between authors.

REFERENCES

1. Le TT, Andreadakis Z, Kumar A, Roman RG, Tollefsen S, Saville M, et al. The COVID-19 vaccine development landscape. Nat Rev Drug Discov. 2020; 19(5):305-306.
2. Siegel RL, Miller KD, Fuchs HE, Jemal A. Cancer statistics, 2022. CA Cancer J Clin. 2022.
3. Zugazagoitia J, Guedes C, Ponce S, Ferrer I, Molina-Pinelo S, Paz-Ares L. Current Challenges in Cancer Treatment. Clin Ther. 2016;38(7):1551-1566.
4. Vasan N, Baselga J, Hyman DM. A view on drug resistance in cancer. *Nature*. 2019;575(7782):299-309.
5. Hassan S, Shehzad A, Khan SA, Miran W, Khan S, Lee YS. Diagnostic and Therapeutic Potential of Circulating-Free DNA and Cell-Free RNA in Cancer Management. Biomedicines. 2022;10(8):2047.
5. Islam SU, Ahmed MB, Ahsan H, Islam M, Shehzad A, Sonn JK, et al. An Update on the Role of Dietary Phytochemicals in Human Skin Cancer: New Insights into Molecular Mechanisms. Antioxidants (Basel). 2020;9(10):916.
6. Bai R, Chen N, Li L, Du N, Bai L, Lv Z, et al. Mechanisms of Cancer Resistance to Immunotherapy. Front Oncol. 2020;10:1290.
7. Islam S.U, Ahmed MB, Lee SJ, Shehzad A, Sonn JK, Kwon OS, et al. PRP4 kinase induces actin rearrangement and epithelial-mesenchymal transition through modulation of the actin-binding protein cofilin. Exp Cell Res. 2018. 369(1):158-165.
8. Islam SU, Ul-Islam M, Ahsan H, Ahmed MB, Shehzad A, Atiya F, et al. Potential applications of bacterial cellulose and its composites for cancer treatment. Int J Biol Macromol. 2021;168:301-309.
9. Azharuddin M , Zhu GH , Das D ,Ozgur E, Uzun L, Turner APF, et al. A repertoire of biomedical applications of noble metal nanoparticles. Chem Commun (Camb). 2019;55(49):6964-6996.
10. Islam SU, Ahmed MB, Islam MU, Shehzad A, Lee YS. Switching from Conventional to Nano-natural Phytochemicals to Prevent and Treat Cancers: Special Emphasis on Resveratrol. Curr Pharm Des. 2019;25(34):3620-3632.
11. Islam SU, Lee JH, Shehzad A, Ahn EM, Lee YM, Lee YS. Decursinol Angelate Inhibits LPS-Induced Macrophage Polarization through Modulation of the NFκB and MAPK Signaling Pathways. Molecules. 2018;23(8):1880.
12. Etter EL, Mei KC, Nguyen J. Delivering more for less: Nanosized, minimal-carrier and pharmacoactive drug delivery systems. Adv Drug Deliv Rev. 2021;179:113994.
13. Unsoy G, Gunduz U. Smart Drug Delivery Systems in Cancer Therapy. *Curr Drug Targets*. 2018;19(3):202-212.
14. Janjua KA, Shehzad A, Shahzad R, Islam SU, Islam MU. Nanocurcumin: A Double-Edged Sword for Microcancers. Curr Pharm Des. 2020;26(45):5783-5792.
15. Kazmi Z, Zeeshan S, Khan A, Malik S, Shehzad A, Seo EK, et al. Anti-epileptic activity of daidzin in PTZ-induced mice model by targeting oxidative stress and BDNF/VEGF signaling. Neurotoxicology. 2020;79:150-163.
16. Khan AU, Khan A, Khan A, Shal B, Aziz A, Ahmed MN, et al. Inhibition of NF-κB signaling and HSP70/HSP90 proteins by newly synthesized hydrazide derivatives in arthritis model [retracted in: Naunyn Schmiedebergs Arch Pharmacol. 2023 Nov;396(11):3341]. Naunyn Schmiedebergs Arch Pharmacol. 2021;394(7):1497-1519.
17. Zhang XF, Liu ZG, Shen W, Gurunathan S. Silver Nanoparticles: Synthesis, Characterization, Properties, Applications, and Therapeutic Approaches. Int J Mol Sci. 2016;17(9):1534.
18. Liu X, Chen JL, Yang WY, Qian YC, Pan JY, Zhu CN, et al. Biosynthesis of silver nanoparticles with antimicrobial and anticancer properties using two novel yeasts. Sci Rep. 2021;11(1):15795.
19. Khan FA, Lammari N, Muhammad Siar AS, Alkhater KM, Asiri S, Akhtar S, et al. Quantum dots encapsulated with curcumin inhibit the growth of colon cancer, breast cancer and bacterial cells. Nanomedicine (Lond). 2020;15(10):969-980.
20. Shehzad A, Qureshi M, Jabeen S, Ahmed R, Alabdalall AH, Aljafary MA, et al. Synthesis, characterization and antibacterial activity of silver nanoparticles using Rhazya stricta. PeerJ. 2018;6:e6086.
21. Albeshri A, Baeshen NA, Bouback TA, Aljaddawi AA. A Review of Rhazya strictaDecne Phytochemistry, Bioactivities, Pharmacological Activities, Toxicity, and Folkloric Medicinal Uses. Plants (Basel). 2021;10(11):2508.
22. Ali BH, Al-Qarawi AA, Bashir AK, Tanira MO. Phytochemistry, pharmacology and toxicity of Rhazya stricta decne: A review. Phytother Res. 2000;14(4):229-234.
23. Ullah, I. A review of phytochemistry, bioactivities and ethno medicinal uses of Rhazya stricta Decsne (Apocynaceae). Af J Microbiol Rese. 2012;6:1629-1641.
24. Gilani SA, Kikuchi A, Shinwari ZK, Khattak ZI, Watanabe KN. Phytochemical, pharmacological and ethnobotanical studies of Rhazya stricta Decne. Phytother Res. 2007;21(4):301-307.
25. Ravinayagam V, Shehzad A, Almohazey D, Almofty S, Jafary MA, AlhAMED N, et al., Decursin induces apoptosis by regulating AMP-activated protein kinase and Bax/Bcl-2 pathway in HepG2 cell line. European Journal of Integrative Medicine, 2018;24:17-22.
26. Shahzad R, Shehzad A, Bilal S, Lee IJ. *Bacillus amyloliquefaciens* RWL-1 as a New Potential Strain for Augmenting Biochemical and Nutritional Composition of Fermented Soybean. *Molecules*. 2020;25(10):2346.
27. Bawazeer S, Rauf A, Emran TB, Aljohani ASM, Alhumaydhi FA, Khan Z, et al., Biogenic synthesis of silver nanoparticles using rhazya stricta extracts and evaluation of its biological activities. Journal of Nanomaterials. 2022;2022.

28. Nadeem AY, Shehzad A, Islam SU, Al-Suhaimi EA, Lee YS. Mosquirix™ RTS, S/AS01 Vaccine Development, Immunogenicity, and Efficacy. *Vaccines (Basel)*. 2022;10(5):713.
29. Zhao C, Dong H, Xu Q, Zhang Y. Histone deacetylase (HDAC) inhibitors in cancer: a patent review (2017-present). Expert Opin Ther Pat. 2020;30(4):263-274.
30. Chaudhuri S, Fowler MJ, Baker C, Stopka SA, Regaan MS, Sablaaatura L, et al. β-Cyclodextrin-poly (β-Amino Ester) Nanoparticles Are a Generalizable Strategy for High Loading and Sustained Release of HDAC Inhibitors. ACS Appl Mater Interfaces. 2021;13(18):20960-20973.
31. Shehzad, A., Curcumin potential and problems in pancreatic cancer. Pancreat Disorders Ther. 2021; 11: S6.
32. Shehzad A, Islam SU, Shahzad R, Khan S, Lee YS. Extracellular vesicles in cancer diagnostics and therapeutics. Pharmacol Ther. 2021;223:107806.
33. Eleutherakis-Papaiakovou E, Kanellias N, Kastritis E, Gavriatopoulou M, Terpos E, Dimopoulos MA. Efficacy of Panobinostat for the Treatment of Multiple Myeloma. J Oncol. 2020;2020:7131802.
34. Sivaraj D, Green MM, Gasparetto C. Panobinostat for the management of multiple myeloma. Future Oncol. 2017;13(6):477-488.
35. Shehzad A, Ravinayagam V, AlRumaih H, Aljafary M, Almohazey D, Almofty S, et al. Application of Three-dimensional (3D) Tumor Cell Culture Systems and Mechanism of Drug Resistance. Curr Pharm Des. 2019;25(34):3599-3607.
36. Shehzad A, Rehmat S, Ul-Islam S, Ahmaad R, Aljafary M, Alrushaid NA, et al. Lirioresinol B dimethyl ether inhibits NF-κB and COX-2 and activates IκBα expression in CCl4-induced hepatic fibrosis. BMC Complement Med Ther. 2020;20(1):49.
37. Shabestarian H, Tabrizi MH, Movehedi M, Neamati Ali, Sharifnia F. Green synthesis of Ag-NPs as a metal nanoparticle and ZnO-NPs as a metal oxide nanoparticle: Evaluation of the in vitrocytotoxicity, anti-oxidant, anti-angiogenic activities. Nanomed J. 2023;10(3):245-258.
38. Azimi F, Mahmoudi F, Mahmoudi F, Amini. MM. Synthesis of silver nanoparticles by Galega officinalis and its hypoglycemic effects in type 1 diabetic rats. Nanomed J. 2021;8(4):255-263.
39. Campoy AHG, Jeronimo FM, Gutierrez RMP, Ramirez AM. Silver nanoparticles synthesized with a fraction from the bark of Eysenhardtia polystachya with high chalcone and dihydrochalcone content effectively inhibit oxidative stress in the zebrafish embryo model. Nanomed J. 2018; 5(3):152-162.
40. Anandalakshmi K. Venugobal J, Ramasamy V. Characterization of silver nanoparticles by green synthesis method using *Pedalium murex* leaf extract and their antibacterial activity. Appl Nanosci 2016;6:399–408.
41. Rezazadeh NH, Buazar F, Matroodi S. Synergistic effects of combinatorial chitosan and polyphenol biomolecules on enhanced antibacterial activity of biofunctionalaized silver nanoparticles. Sci Rep. 2020;10(1):19615.
42. Sadat Shandiz SA, Shafiee Ardestani M, Shahbazzadeh D, Assadi A, Cohan RA, Asgary V, et al. Novel imatinib-loaded silver nanoparticles for enhanced apoptosis of human breast cancer MCF-7 cells. Artif Cells Nanomed Biotechnol. 2017;45(6):1-10.
43. Tan JM, Karthivashan G, Gani SA, Fakurazi S, Hussein MZ. *In vitro* drug release characteristic and cytotoxic activity of silibinin-loaded single walled carbon nanotubes functionalized with biocompatible polymers. Chem Cent J. 2016;10:81.